J Mater Sci (2009) 44:1858–1867
DOI 10.1007/s10853-008-3237-2

Preparation, structural characterisation and antibacterial properties of Ga-doped sol–gel phosphate-based glass

D. M. Pickup · S. P. Valappil · R. M. Moss · H. L. Twyman · P. Guerry · M. E. Smith · M. Wilson · J. C. Knowles · R. J. Newport

Received: 22 August 2008 / Accepted: 30 December 2008 / Published online: 3 February 2009

Abstract A sol–gel preparation of Ga-doped phosphate-based glass with potential application in antimicrobial devices has been developed. Samples of composition $(CaO)_{0.30}(Na_2O)_{0.20-x}(Ga_2O_3)_x(P_2O_5)_{0.50}$ where $x = 0$ and 0.03 were prepared, and the structure and properties of the gallium-doped sample compared with those of the sample containing no gallium. Analysis of the ^{31}P MAS NMR data demonstrated that addition of gallium to the sol–gel reaction increases the connectivity of the phosphate network at the expense of hydroxyl groups. This premise is supported by the results of the elemental analysis, which showed that the gallium-free sample contains significantly more hydrogen and by FTIR spectroscopy, which revealed a higher concentration of –OH groups in that sample. Ga K-edge extended X-ray absorption fine structure and X-ray absorption near-edge structure data revealed that the gallium ions are coordinated by six oxygen atoms. In agreement with the X-ray absorption data, the high-energy XRD results also suggest that the Ga^{3+} ions are octahedrally coordinated with respect to oxygen. Antimicrobial studies demonstrated that the sample containing Ga^{3+} ions had significant activity against *Staphylococcus aureus* compared to the control.

D. M. Pickup (✉) · R. M. Moss · H. L. Twyman · R. J. Newport
School of Physical Sciences, University of Kent, Canterbury CT2 7NH, UK
e-mail: dmp@kent.ac.uk

S. P. Valappil · J. C. Knowles
Division of Biomaterials and Tissue Engineering, UCL Eastman Dental Institute, London WC1X 8LD, UK

P. Guerry · M. E. Smith
Department of Physics, University of Warwick, Coventry CV4 7AL, UK

M. Wilson
Division of Microbial Diseases, UCL Eastman Dental Institute, London WC1X 8LD, UK

Introduction

The emergence of multi-resistant nosocomial pathogens such as *MRSA* and *Clostridium difficile* and the lack of new antibacterial drugs and antibiotics in the advanced stages of development underlie the need to find more effective antimicrobial agents [1]. A recent study has found that Ga^{3+} ions inhibit *Pseudomonas aeruginosa* growth and biofilm formation, and kill planktonic and biofilm bacteria in vitro by decreasing bacterial Fe uptake and by interfering with Fe signalling by the transcriptional regulator *pvdS* [2]. It was also shown that gallium is effective in two murine lung infection models. Other studies have demonstrated that gallium is effective against the organisms causing tuberculosis [3] and malaria [4] in human beings, and in the treatment of *Rhodococcus equi* caused pneumonia in foals [5].

Recently, we have shown that phosphate-based glasses (PBGs) in the $CaO–Na_2O–P_2O_5$ system provide a means to deliver Ga^{3+} ions in a controlled way [6]. PBGs have predictable dissolution rates that can be manipulated via chemical composition to give materials that degrade over a period of a few hours to those that are stable for over 1 year. Furthermore, PBGs containing calcium and sodium are both biocompatible and bioresorbable [7]. Since the release of active ions incorporated into the glass structure is controlled by the overall dissolution rate of the glass, which is often linear with time, this system has been

extensively studied over recent years for use in controlled-delivery devices for biomedical applications [8]. PBGs containing Cu and Ag ions have been investigated as antimicrobial agents; demonstrating activity against multi-resistant nosocomial pathogens and bacteria residing in biofilms [9–11]. Other applications include oral healthcare, via the release of fluoride ions, and veterinary treatment where glasses are designed to reside in the animals' stomachs and release trace elements slowly over extended periods of time [8]. Testing of the antibacterial properties of the Ga-doped PBG glasses revealed a net bactericidal effect due to Ga^{3+} ions, with a Ga_2O_3 concentration as low as 1 mol.% sufficient to impart potent bactericidal properties. These results suggest that Ga-doped PBG is a potentially promising new therapeutic agent for pathogenic bacteria including *MRSA* and *C. difficile* [6].

Here, we have prepared Ga-doped PBG by a sol–gel route, which, to the best of our knowledge, is the first report of such a preparation. The method is based upon that which we developed to prepare biocompatible, bioresorbable, sol–gel $(CaO)_{0.3}(Na_2O)_{0.2}(P_2O_5)_{0.5}$ glass [12] with the addition of gallium ethoxide as the Ga^{3+} precursor. The sol–gel method has some advantages over traditional melt-quenching approaches in biomedical applications; the most notable of which are the low temperature nature of the preparation, which allows scope for the encapsulation of drugs into the biomaterial, and the potential to coat biomedical devices using sol–gel processing to improve their properties, e.g. a hydroxyapatite layer to improve bonding to bone [13].

We also report the characterisation of the new Ga-doped PBG sol–gel. We have studied the structure using synchrotron X-ray techniques, infrared spectroscopy and solid-state NMR, and measured the antibacterial activity against *Staphylococcus aureus*. The results have been compared to those from a similar sample containing no gallium.

Materials and methods

Sample preparation

The following precursors were used, without further purification, in the sol–gel preparation: 1:1 molar mixture of mono- and di-substituted *n*-butyl phosphate ($OP(OH)_2(OBu^n)$ and $OP(OH)(OBu^n)_2$, Alfa Aesar, ~98%), sodium methoxide solution (NaOMe, Aldrich, 30 wt% in methanol), calcium methoxyethoxide solution (Ca-methoxyethoxide, 17.5 wt% in methoxyethanol) and gallium ethoxide (Alfa Aesar). The Ca-methoxyethoxide solution was prepared by reacting the appropriate amount of calcium metal (Riedel-de Haën, 98%) with 2-methoxyethanol (Aldrich, 99.8%) under argon at 80 °C for 24 h. The concentration of the resultant solution was confirmed gravimetrically by evaporating the solvent and heating to 1,050 °C for 12 h to convert the alkoxide to CaO.

The sol–gel preparation of the gallium-doped sample is outlined by the flowchart in Fig. 1. The *n*-butyl phosphate was first added dropwise using a syringe through a septum to a vessel containing the NaOMe solution: the solution was stirred magnetically throughout this addition. After 1 h, the Ca-methoxyethoxide solution was added using the same method. The gallium ethoxide was also added via syringe after a further 10 min of stirring. The sol was then allowed to gel, which typically took ~2 h, and left overnight. During this period, the gel liquefied, allowing the resultant sol to be cast in a polypropylene container. This sol was aged at 60 °C for 1 week, during which time the final gellation occurred, before drying at 120 °C for 2 weeks. The dried gel was heated to 250 °C to remove solvent, water and organic molecules. The sample containing no gallium was prepared by the same method except that no gallium ethoxide was added [12]. Samples of nominal composition $(CaO)_{0.30}(Na_2O)_{0.20-x}(Ga_2O_3)_x(P_2O_5)_{0.50}$ where $x = 0$ and 0.03 were prepared: for simplicity, we refer hereafter to these samples as 0Ga-PBG and 3Ga-PBG, respectively.

Characterisation necessary for a quantitative analysis of the X-ray diffraction data was performed: elemental analysis (ICP-AES and combustion) was carried out by a commercial company (Medac Ltd) and macroscopic densities were

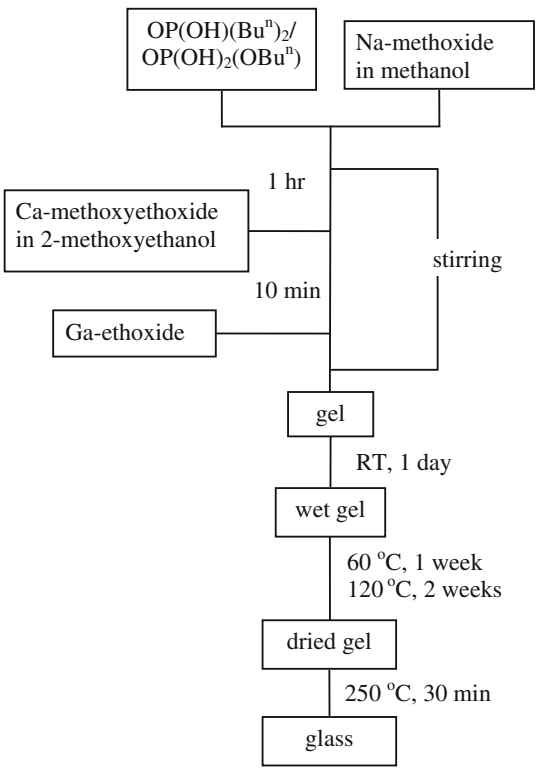

Fig. 1 Flow diagram of the sol–gel preparation

determined by helium pycnometry using a Quantachrome Multipycnometer. The elemental analysis revealed that the compositions of the oxide components of the 0Ga-PBG and 3Ga-PBG samples were $(CaO)_{0.28}(Na_2O)_{0.21}(P_2O_5)_{0.51}$ and $(CaO)_{0.26}(Na_2O)_{0.16}(Ga_2O_3)_{0.03}(P_2O_5)_{0.55}$, respectively. As expected with sol–gel samples, some residual carbon and hydrogen were also detected: the sample with no gallium contained 3.6 wt% C and 1.1 wt% H, whereas the sample with 3 mol.% Ga_2O_3 contained 1.7 wt% C and 0.7 wt% H.

Solid state NMR

^{31}P NMR experiments were carried out on a CMX Infinity spectrometer attached to an 8.45 T magnet giving a ^{31}P Larmor frequency of 145.77 MHz. Samples were placed in the magnet using a Doty 4 mm MAS probe and spun at 12 kHz. The associated Spinsight software was used to run one-pulse experiments with a 2.7 μs pulse length corresponding to a $\pi/6$ tip angle, with a pre-acquisition delay of 10 μs. A 20 s repetition time was used and no saturation was observed. Typically, 150 scans were accumulated to obtain a good signal-to-noise ratio. Spectra were referenced to the resonance of the secondary reference ammonium dihydrogen phosphate ($NH_4H_2PO_4$) at 0.9 ppm (relative to 85% H_3PO_4 solution at 0 ppm).

Fourier transform infrared (FTIR) spectroscopy

Infrared spectra were recorded in transmission mode on a Biorad FTS175C spectrometer controlled by Win-IR software. Samples ($\sim$1 mg) were diluted in dry KBr (250 mg) and scanned in the range 4,000–450 cm^{-1} with a resolution of 4 cm^{-1}. Each spectrum was the result of summing 64 scans.

Ga K-edge X-ray absorption spectroscopy (XAS)

Ga K-edge XAS measurements were made at room temperature on Station 16.5 at the SRS, Daresbury Laboratory, UK, with a ring energy of 2 GeV and a stored current of 150–250 mA. The spectra were recorded in transmission mode using a double crystal Si(220) monochromator ($d = 1.92$ Å) and ionisation chambers to detect the incident and transmitted beam intensities. Finely ground samples were diluted in polyethylene (Aldrich, spectrophotometric grade) and pressed into pellets to give a satisfactory edge step and absorption. An encapsulated gallium foil and a third ionisation chamber were placed after the sample to allow an absorption spectrum of the foil to be collected simultaneously for the purpose of calibration of the energy scale. The energy scale was defined by assigning the point of maximum gradient on the absorption edge from the Ga foil to 10367 eV.

X-ray absorption near-edge structure (XANES) spectra were collected from 50 eV below to 175 eV above the Ga K-edge in order to allow accurate background subtraction. A fine energy step of 0.4 eV was used around the edge. The data processing comprised conversion of the data to absorption versus energy, calibration of the energy scale, removal of the pre-edge background by straight-line fitting and removal of the post-edge background by fitting with a polynomial. All the spectra were normalised to have an edge-step of 1. As well as the data from the gallium-doped PBG, spectra were also collected from a series of crystalline reference materials containing Ga^{3+} ions in well-defined coordination geometries: quartz α-$GaPO_4$, β-Ga_2O_3, $Ga_2(SO_4)_3$ and $Ga(acac)_3$. The $Ga(acac)_3$ (Aldrich, 99.99%) and $Ga_2(SO_4)_3$ (Aldrich, 99.995%) were purchased commercially, whilst the quartz α-$GaPO_4$ and β-Ga_2O_3 were synthesised. The quartz α-$GaPO_4$ was prepared by precipitation from an aqueous mixture of $GaCl_3$ (Aldrich, 99.99%) and H_3PO_4 by the addition of NH_4OH. The product was separated by filtration, washed and dried before heating to 800 °C to remove ammonium and hydroxyl groups [14]. The β-Ga_2O_3 was prepared by calcination of Aldrich 99.99% Ga_2O_3 overnight at 1,000 °C [15]. The gallium foil used for the calibration of the energy scale was prepared by hot-pressing Aldrich 99.99% Ga metal between two sheets of filter paper and laminating the resultant construct in plastic.

Extended X-ray absorption fine structure (EXAFS) data spectra were collected over the range $k = 3$–14 $Å^{-1}$ with a step of 0.04 $Å^{-1}$ and a counting time of 1–10 s per point varying as k^3 ($k = \sqrt{2m_e/\hbar^2(E - E_0)}$, where m_e is the rest mass of the electron, E the energy and E_0 the energy of the absorption edge). The programs EXCALIB, EXSPLINE and EXCURV98 [16] were used to extract the EXAFS signal and analyse the data. Least squares refinements of the structural parameters were carried out against the k^3-weighted EXAFS signal to minimise the fit index, FI,

$$\mathrm{FI} = \sum_i \left(k^3(\chi_i^{\mathrm{T}} - \chi_i^{\mathrm{E}})\right)^2 \quad (1)$$

where χ_i^{T} and χ_i^{E} are the theoretical and experimental EXAFS, respectively. The results of the refinements are reported in terms of the discrepancy index, R_{di}

$$R_{\mathrm{di}} = \frac{\int |(\chi^{\mathrm{T}}(k) - \chi^{\mathrm{E}}(k))|k^3 \mathrm{d}k}{\int |\chi^{\mathrm{E}}(k)|k^3 \mathrm{d}k} \times 100\%. \quad (2)$$

Quartz α-$GaPO_4$ was run as a reference material to check the validity of our data analysis and also to allow refinement of the parameter *AFAC* (defined as the proportion of the photo-electrons taking part in an 'EXAFS-type' scattering event). *AFAC* was refined together with the Ga–O and Ga–P distances with the associated coordination numbers fixed at crystallographic values obtained from the literature [17, 18].

High-energy XRD (HEXRD)

High-energy XRD data were collected on Station 9.1 at the Synchrotron Radiation Source (SRS), Daresbury Laboratory, UK. The finely powdered samples were enclosed inside a 0.5-mm thick circular metal annulus by kapton windows and mounted onto a flat-plate instrumental set-up. The wavelength was set at $\lambda = 0.4858$ Å and calibrated using the K-edge of an Ag foil; this value was low enough to provide data to a high value of momentum transfer ($Q_{max} = 4\pi\sin\theta/\lambda \sim 23$ Å^{-1}). The data were reduced using a suite of programs written in-house: the initial stage of analysis of XRD data from an amorphous material involves the normalisation, removal of background scattering, correction for absorption and Compton (inelastic) scattering, and subtraction of the self-scattering term [19]. The resultant scattered intensity, $i(Q)$, can reveal structural information by Fourier transformation to obtain the pair-distribution function:

$$T(r) = T^0(r) + \int_0^\infty Qi(Q)M(Q)\sin(Qr)\mathrm{d}Q \quad (3)$$

where $T^0(r) = 2\,\pi^2 r\,\rho_o$ (r is the atomic separation between atoms and ρ_o is the macroscopic number density) and $M(Q)$ is a window function necessitated by the finite maximum experimentally attainable value of Q.

Structural information can be obtained from the diffraction data by modelling the Q-space data and converting the results to r-space by Fourier transformation to allow comparison with the experimentally determined pair-distribution function [20]. The structural parameters used to generate the Q-space simulation are varied to optimise the fit to the experimental data. The Q-space simulation is generated using the following equation:

$$p(Q)_{ij} = \frac{N_{ij}w_{ij}}{c_j}\frac{\sin QR_{ij}}{QR_{ij}}\exp\left[\frac{-Q^2\sigma_{ij}^2}{2}\right] \quad (4)$$

where $p(Q)_{ij}$ is the pair function in reciprocal space, N_{ij}, R_{ij} and σ_{ij} are the coordination number, atomic separation and disorder parameter, respectively, of atom i with respect to j, c_j is the concentration of atom j and w_{ij} is the weighting factor. The weighting factors are given by:

$$w_{ij} = \frac{2c_ic_jf(Q)_if(Q)_j}{\overline{f(Q)}^2} \text{ if } i \neq j \quad (5)$$

or,

$$w_{ij} = \frac{c_i^2f(Q)_i^2}{\overline{f(Q)}^2} \text{ if } i = j \quad (6)$$

where $f(Q)$ represents the Q-dependant X-ray form factors.

The errors associated with the HEXRD data arise mainly from the fitting process due to the problem of overlapping correlation shells. They have been estimated from the tolerance that a particular parameter may have without significantly changing the overall quality-of-fit. Some additional systematic error may result from the data reduction process but these are expected to be small compared to those arising from the simulation of the experimental data.

Antibacterial growth assay

The sol–gel prepared 0Ga-PBG and 3Ga-PBG glasses were investigated for their ability to inhibit bacterial growth using a disc-diffusion methodology (BSAC Disk Diffusion Method for Antimicrobial Susceptibility Testing, Version 4, 2005). Isosensitest agar (Oxoid, Basingstoke, UK) plates were inoculated with a standardised culture of *S. aureus* (NCTC 6571). One hundred milligrams of both control and gallium-containing PBGs were placed in the middle of the inoculated plates. The experiment was conducted in triplicate and the glasses not containing any gallium were used as negative controls. These plates were then incubated overnight in air at 37 °C. The diameters of any zones that had formed around the glass samples were measured using callipers.

Results

Solid state NMR data

The ^{31}P MAS NMR spectra from the two samples studied are shown in Fig. 2. Also shown is the fits to the spectra obtained by Gaussian deconvolution; this deconvolution process included fitting the spinning side-bands, which are not shown in the figure. The results of the Gaussian deconvolution are given in Table 1.

It can be seen from the results in Table 1 that three peaks can be resolved in both spectra. The resonances in ^{31}P NMR spectra from PBGs are normally assigned to Q^n phosphorus sites, where n represents the number of bridging oxygen atoms in the PO_4^{3-} group, which connect to other such phosphate tetrahedra [21, 22]. On the basis of previous work in the literature [12, 21, 22], the resonances observed here at around −1, −10 and −23 ppm are assigned to Q^0, Q^1 and Q^2 phosphorus environments, respectively. The NMR spectrum from the 0Ga-PBG sample features an additional very sharp peak at −1.5 ppm. A similar resonance was observed previously in the ^{31}P NMR spectrum from sol–gel prepared CaO–Na_2O–P_2O_5 glass and assigned to unreacted monomeric phosphates (e.g. $OP(OH)_{3-x}(OBu^n)_x$) [12]. The narrowness of this

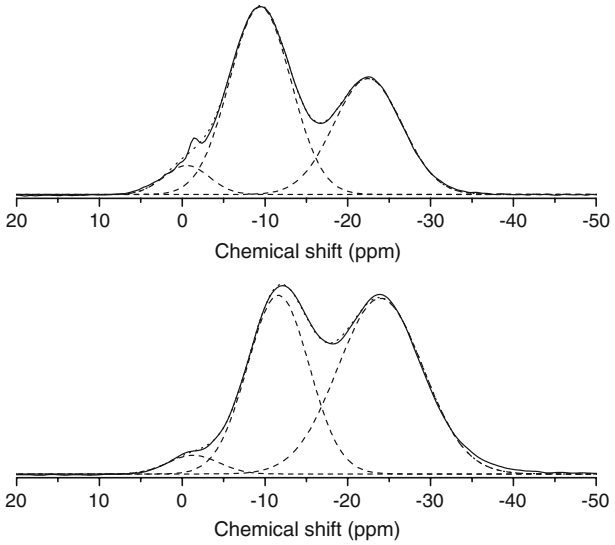

Fig. 2 ^{31}P MAS NMR spectra from 0Ga-PBG (*top*) and 3Ga-PBG sol–gel glasses (*bottom*) including their Gaussian deconvolution. The data are represented by a *solid line*, the overall fit by a *dotted line* and the individual Gaussian contributions by *dashed lines*

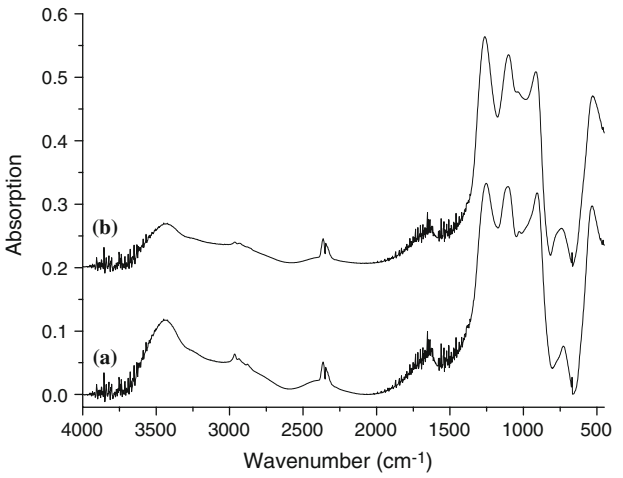

Fig. 3 FTIR spectra from the sol-gel glasses: (a) 0Ga-PBG sample and (b) 3Ga-PBG sample

resonance suggests that these monomeric phosphates are either more ordered in this sample or partially mobile. The relative intensity of this resonance was considered small enough for it to be excluded from the fitting process.

FTIR spectroscopy

The FTIR spectra from the sol–gel glass samples are shown in Fig. 3. The absorption bands have been assigned according to the literature [23–26]. The broad band in the region 3,600–3,000 cm^{-1} is due to the fundamental vibrations of hydroxyl groups [27]. The band near 1,250 cm^{-1} is assigned to the asymmetric stretching mode of the two non-bridging oxygen atoms bonded to phosphorus atoms in the Q^2 tetrahedral sites, $\nu_{as}(PO_2)^-$. The absorption bands close to 1,100 and 1,000 cm^{-1} are assigned to the asymmetric and symmetric stretching modes of chain-terminating Q^1 groups ($\nu_{as}(PO_3)^{2-}$ and $\nu_s(PO_3)^{2-}$), respectively. The absorption band near 900 cm^{-1} is assigned to the asymmetric stretching modes of the P–O–P linkages, ν_{as}(P–O–P), and the partially split band centred around 750 cm^{-1} is assigned to the symmetric stretching modes of these linkages, ν_s(P–O–P). The peak at 540 cm^{-1} is attributed to O–P–O deformation modes.

Ga K-edge X-ray absorption spectroscopy

The Ga K-edge XANES spectra from the reference materials and the 3Ga-PBG sol–gel glass are shown in Fig. 4. Different gallium coordination sites can be distinguished using Ga K-edge XANES by comparison of the spectra with those from materials containing Ga^{3+} in well-defined structural sites [15, 28, 29]. Here, we chose reference materials with a range of gallium coordination environments: quartz α-$GaPO_4$ contains tetrahedrally coordinated gallium [14], β-Ga_2O_3 an equal mixture of tetrahedral and octahedral gallium [28], and $Ga(acac)_3$ and $Ga_2(SO_4)_3$ octahedral gallium [28, 30]. Figure 4 shows that for the octahedrally coordinated gallium a broad feature at $\sim$10377 eV is observed, whilst for the tetrahedrally coordinated gallium a sharper peak is seen at slightly lower energy (10375.8 eV) together with a broader feature at higher energy (10384.5 eV). The spectrum from the mixed-site material, β-Ga_2O_3, is consistent with a combination of the features observed for both the single-site materials.

Table 1 Results of the deconvolution of the ^{31}P MAS NMR spectra from the 0Ga-PBG and 3Ga-PBG sol–gel glasses using Gaussian functions

Sample	Assignment	Chemical shift (ppm) (±1.0 ppm)	Width (ppm) (±1.0 ppm)	Relative intensity (%) (±2.0%)
0Ga-PBG	Q^0	−0.5	5.5	5
	Q^1	−9.4	7.4	53
	Q^2	−22.4	8.2	42
3Ga-PBG	Q^0	−1.4	6.1	3
	Q^1	−11.6	7.4	38
	Q^2	−23.9	10.3	59

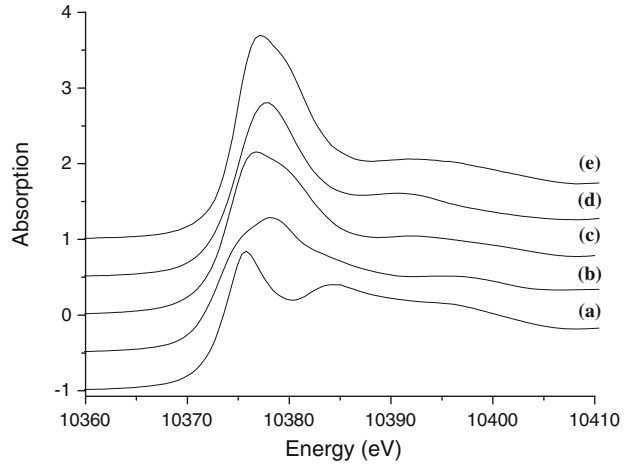

Fig. 4 Ga K-edge XANES spectra: (a) quartz α-$GaPO_4$, (b) β-Ga_2O_3, (c) $Ga_2(SO_4)_3$, (d) $Ga(acac)_3$ and (e) 3Ga-PBG sol–gel glass

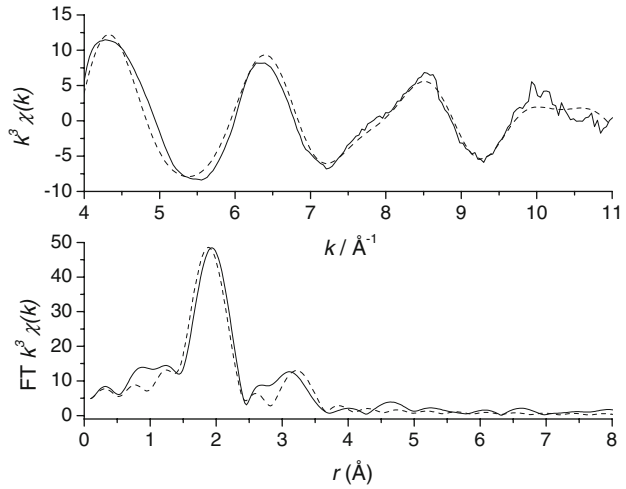

Fig. 5 Ga K-edge EXAFS data from the 3Ga-PBG sol–gel glass: k^3-weighted EXAFS (*top*) and Fourier transform (*bottom*). Experimental data, *solid line*, and theoretical fit, *dotted line*

These qualitative observations are in agreement with those of previous studies [15, 28].

Figure 5 shows the EXAFS data from the 3Ga-PBG sol–gel glass; both *k*-space data and their Fourier transform are shown together with the calculated fits. The Fourier transform exhibits two peaks at ~2 and 3.2 Å, which are assigned, by comparison with the atomic distances found in crystalline gallium phosphates [17], to Ga–O and Ga–P distances, respectively. The structural parameters obtained from the fitting of the EXAFS data from both the Ga-doped sol–gel and the $GaPO_4$ reference material using curved wave theory are given in Table 2.

HEXRD data

Figures 6 and 7 show the HEXRD data from the 0Ga-PBG and 3Ga-PBG sol–gel samples, respectively. Both the *r*-space and *Q*-space data are shown together with the fits to the pair-distribution functions obtained using the method described above. The structural parameters obtained from the fitting of the HEXRD data are given in Table 3. The peaks have been assigned according to the results of previous studies and by comparison with crystals [17, 31, 32].

Antimicrobial activity

The results of the disc-diffusion study of the antimicrobial activity of the Ga-doped sample against *S. aureus* are shown in Fig. 8; the sample containing no gallium was used as the control. The zones of inhibition (i.e. zones of no visible bacterial growth surrounding the glasses) were found to be approximately five times larger in diameter for the gallium-containing glass when tested against *S. aureus* compared to the same glass with no gallium.

Discussion

Structural characterisation

It is generally accepted that PBGs close to the metaphosphate composition, i.e. those having an atomic ratio of phosphorus to oxygen (O/P) of close to three, have structures comprised rings and chains of PO_4^{3-} tetrahedra [33]. The oxygen atoms of the phosphate tetrahedra can either be classed as bridging oxygens (BOs) if they connect to other phosphate groups or as non-bridging oxygens (NBOs) if they coordinate cations. ^{31}P MAS NMR provides information on the connectivity of the phosphate units by

Table 2 Ga K-edge EXAFS-derived structural parameters

Sample	Shell	*N*	*R* (Å)	*A* ($Å^{-2}$)	R_{di} (%)	Crystallographic data (Å)
Quartz α-$GaPO_4$	Ga–O	*4*	1.81(2)	0.005(1)	32.6	4 × 1.82
	Ga···P	*8*	3.12(2)	0.030(4)		8 × 3.09
3 mol% Ga_2O_3 sol–gel glass	Ga–O	6.9(5)	1.94(2)	0.013(2)	23.8	N/A
	Ga···P	1.8(8)	3.18(2)	0.005(2)		

Note that the numbers in italics were fixed during the refinement. The crystallographic parameters were taken from reference [18]

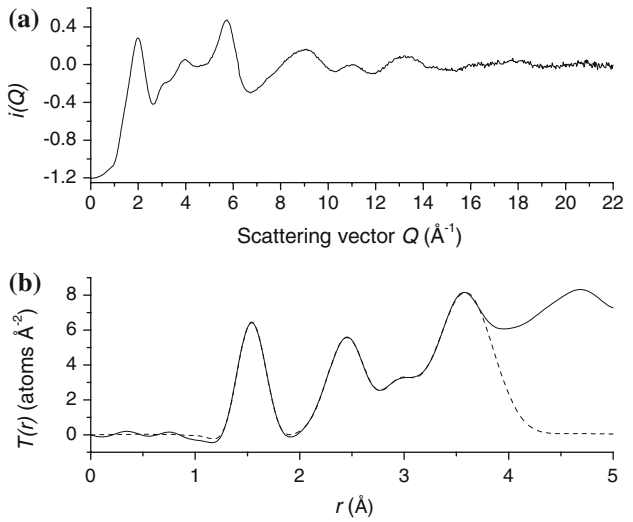

Fig. 6 X-ray diffraction data from the 0Ga-PBG sol–gel glass: **a** Q-space interference function, $i(Q)$, and **b** pair-distribution function, $T(r)$, (*solid line*) together with fit (*dashed line*)

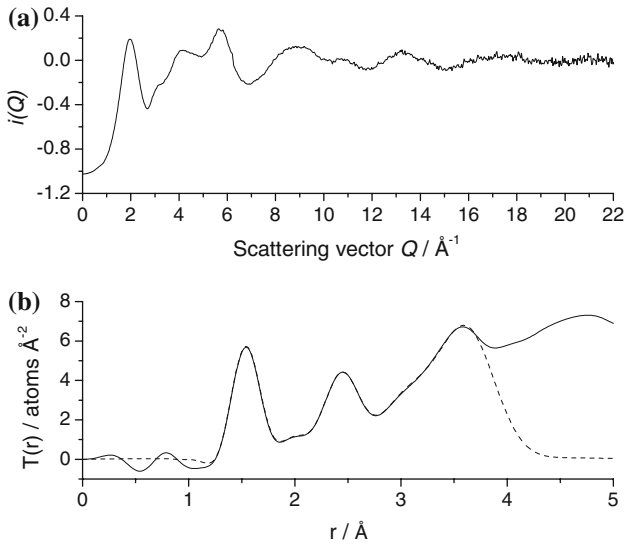

Fig. 7 X-ray diffraction data from the 3Ga-PBG sol–gel glass: **a** Q-space interference function, $i(Q)$, and **b** pair-distribution function, $T(r)$, (*solid line*) together with fit (*dashed line*)

revealing the relative concentrations of the various Q^n species present. The results in Table 1 show that the sol–gel glasses here have structures consisting mainly of Q^1 and Q^2 phosphate units with a small proportion ($\sim$5%) of Q^0 groups. This type of Q^n distribution is typical of sol–gel prepared PBGs and contrasts with that of analogous melt-quenched glasses [12]. A melt-quenched glass of nominal composition $(CaO)_{0.20}(Na_2O)_{0.20}(P_2O_5)_{0.50}$ has an O/P ratio of close to 3 and as such is expected to have a structure consisting of entirely Q^2 units [21]: in close agreement with this prediction, it has been shown experimentally that the structure of this glass consists of 95% Q^2 [12]. The

Table 3 Structural parameters obtained from the simulation of the HEXRD data

Sample	Density (g/cm^3)	Correlation	R (Å)	N	σ (Å)
0Ga-PBG	2.36	P–NBO	1.49(1)	1.8(2)	0.02(1)
		P–BO	1.60(1)	1.9(2)	0.04(1)
		Ca–O	2.34(2)	4.4(5)	0.08(2)
		Na–O	2.38(2)	5.2(5)	0.07(2)
		O···O	2.54(1)	4.4(4)	0.06(2)
		Ca–O	2.80(2)	1.6(2)	0.12(2)
		P···P	2.95(1)	1.4(1)	0.09(2)
3Ga-PBG	2.42	P–NBO	1.50(1)	1.8(2)	0.02(1)
		P–BO	1.60(1)	1.8(2)	0.07(1)
		Ga–O	1.98(2)	5.9(3)	0.09(2)
		Ca–O	2.36(2)	3.9(5)	0.08(2)
		Na–O	2.38(2)	4.9(5)	0.06(2)
		O···O	2.54(1)	4.4(4)	0.09(2)
		Ca–O	2.76(2)	1.2(2)	0.10(2)
		P···P	2.95(2)	1.5(2)	0.10(2)
		Ga···P	3.18(2)	5.3(5)	0.11(3)

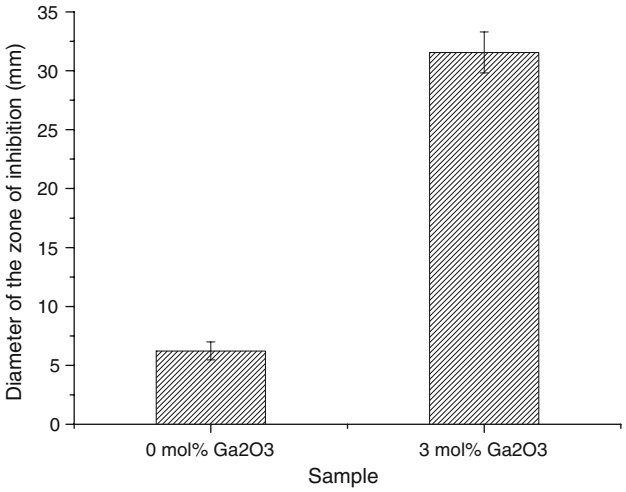

Fig. 8 Results of the disc-diffusion study of antimicrobial activity over a 24-h period against *Staphylococcus aureus*

gallium-free sol–gel sample studied here has the same nominal composition, but has a structure with only 40% Q^2 units. The difference is that the sol–gel glasses contain a significant concentration of hydrogen: this hydrogen is present in the structure as –OH groups, which terminate the phosphate chains and reduce connectivity. In short, the structure of the melt-quenched glass need only have enough NBOs to coordinate and charge-balance the metal cations, whereas its sol–gel counterpart requires extra NBOs to charge balance the H^+ ions.

When considering the structure of sol–gel prepared PBGs, it is useful to use ^{31}P NMR data to calculate the average P···P coordination number (N_{PP}) and the average

phosphate chain length (L). N_{PP} can be calculated from the atomic fractions of Q^1 (f_{Q1}) and Q^2 (f_{Q2}) phosphorus sites in the structure using the equation:

$$N_{PP} = f_{Q1} + 2f_{Q2}. \quad (7)$$

Using this approach, we obtain values of N_{PP} of 1.4 and 1.6 for the 0Ga-PBG and 3Ga-PBG samples, respectively. Similarly, if we assume, for the benefit of the calculation, that the structure consists of only linear phosphate chains with an absence of rings, an average phosphate chain length, L, can be calculated from N_{PP}:

$$L = \frac{-2}{N_{PP} - 2}. \quad (8)$$

Applying Eq. 8, we obtain average phosphate chain lengths of 3.1 and 4.5 for the 0Ga-PBG and 3Ga-PBG samples, respectively. Thus, there is significantly higher connectivity between the phosphate groups in structure of the gallium-containing sample compared to the gallium-free sample resulting in a 50% increase in the average phosphate chain length. This suggests that addition of a small amount of gallium ethoxide to the sol–gel reaction promotes the formation of P–O–P bridges. The reason for this maybe the high reactivity of gallium ethoxide towards hydrolysis, which is due to the high positive charge density on the Ga^{3+} ion [34] and may drive the condensation of P–OH groups by consuming the water that is released. In terms of sol–gel chemistry, this is an important result: in contrast to silicate-based sol–gel reactions where Si–O–Si bonds readily form, it is difficult to get extensive P–O–P bonding in the analogous phosphate-based reactions [35]. As an example, vitreous silica can be easily prepared using sol–gel chemistry, whereas the preparation of vitreous P_2O_5 by the same methods has not been achieved. The increased phosphate connectivity in the 3Ga-PBG sample is further evidenced by the elemental analysis. The 3Ga-PBG sample (0.7 wt%) contains significantly less hydrogen than the gallium-free sample (1.1 wt%), suggesting that the latter sample contains a higher concentration of –OH groups.

The FTIR spectra shown in Fig. 3 provide more direct evidence for the presence of a greater concentration of –OH groups in the structure of the Ga-free sample. The broad absorption at 3,450 cm^{-1} that corresponds to the O–H vibration in P–OH groups [36] is significantly more intense in the spectrum from the 0Ga-PBG sample compared to that from the 3Ga-PBG sample. The other notable difference between the spectra from the two samples is the relative intensities of the peaks at 1,250 and 1,100 cm^{-1}. The peak at 1,250 cm^{-1} is the primary mode associated with the P–O vibrations of Q^2 groups, whereas the band at 1,100 cm^{-1} is the most intense band associated with the P–O modes of Q^1 end groups. The fact that the relative intensity of the 1,250 cm^{-1} band is significantly greater in the spectrum from the 3Ga-PBG sample compared to that from the 0Ga-PBG sample suggests, in agreement with the ^{31}P NMR results, that the abundance of Q^2 species is greater in the structure of the former sample.

The XANES spectrum from the 3Ga-PBG sample exhibits one broad feature, which is similar in shape and position to that observed in the spectra from the reference materials containing octahedral gallium, suggesting that the Ga^{3+} ions in the sol–gel glass adopt this coordination geometry. Of the two reference spectra from the materials containing octahedral gallium, the spectrum from the sol–gel sample is most similar to that from $Ga_2(SO_4)_3$ with the predominant peak displaying slight asymmetry and the absorption maximum occurring at slightly lower energy than observed for $Ga(acac)_3$. Since $Ga(acac)_3$ contains Ga^{3+} ions surrounded by a near perfect octahedron of oxygen atoms [28], whereas the structure of $Ga_2(SO_4)_3$ has two gallium sites, both significantly distorted relative to the ideal octahedral geometry [30], the observations here suggest some degree of distortion around the gallium site in the sol–gel PBG.

The results in Table 2 obtained from the analysis of the EXAFS data reveal that the Ga^{3+} ions in the sol–gel PBG are surrounded by 6.9 oxygen atoms at a distance of 1.94 Å and by 1.8 phosphorus atoms at a distance of 3.18 Å. Given the errors associated with EXAFS derived coordination numbers (typically ±20%), these parameters are entirely consistent with gallium ions adopting octahedral coordination with respect to oxygen. Stronger evidence for the presence of six-fold coordination comes from the measured Ga–O bond distance of 1.94 Å, since Ga–O distances show a strong correlation with coordination number. Typical Ga–O distances for tetrahedral gallium fall in the range 1.82–1.84 Å, those for five coordinate gallium in the range 1.88–1.92 Å and those for octahedral gallium 1.94–1.99 Å [17]. Comparing this result with the few studies of Ga-containing PBG in the literature, we find that octahedral coordination with respect to oxygen is typical in glasses with a high P/Ga ratio [37, 38]. Hoppe et al. [37] studied Ga_2O_3–P_2O_5 melt-quenched glasses with HEXRD and found only GaO_6 octahedra at the metaphosphate composition (P/Ga = 3), whereas at the pyrophosphate composition (P/Ga = 1.5), they found that the majority of Ga^{3+} ions occupied tetrahedral sites. Belkebir et al. [38] used a combination of Ga K-edge EXAFS and ^{71}Ga NMR to study Na_2O–Ga_2O_3–P_2O_5 melt-quenched glasses. Their results suggest that, in the ternary system, once the P/Ga gets to 5 or above all the Ga^{3+} ions adopt octahedral coordination. Since the Ga-doped sol–gel glass at the centre of this study has a P/Ga = 18.3, the presence of GaO_6 octahedra agrees entirely with the trend suggested by the literature. In fact, our own ^{71}Ga NMR study of

$CaO–Na_2O–Ga_2O_3–P_2O_5$ melt-quenched glasses with a P/Ga > 9 detected only octahedral gallium [6].

High-energy X-ray diffraction data gives information on the structure of a material by revealing the correlations between the atoms present. The parameters that define these correlations, i.e. atomic distances, coordination numbers and disorder parameter, are obtained by simulating the data in real space. The results of this process for the 0Ga-PBG and 3Ga-PBG sol–gel samples in Table 2 reveal, not only the environment adopted by the gallium ions in the glass, but also the effect they have on the phosphate network that forms the backbone of the structure. The structural parameters from the 0Ga-PBG sample are typical of a sol–gel phosphate glass containing Ca^{2+} and Na^{+} ions [12]. The P–O coordination number is close to 4, as expected for a structure based on tetrahedral PO_4^{3-} groups, with short and long P–O distances ascribed to bonds to non-bridging and bridging oxygen atoms, respectively [33]. The Ca–O and Na–O distances of ~2.35 Å and coordination numbers of ~6 and ~5, respectively, agree with those measured previously by diffraction for these ions in PBGs [12, 32]. A longer Ca–O distance is also observed at ~2.8 Å suggesting a similar calcium environment to that found in silicate-based sol–gel bioactive glasses [39]. The O···O nearest-neighbour distance of 2.54 Å corresponds to the oxygen–oxygen distance in a PO_4^{3-} tetrahedron (*cf.* calculated value of 2.52 Å assuming a O–P–O bond angle of 109° and a P–O distance of 1.55 Å). The distance of 2.95 Å measured for the P···P correlation represents the phosphorus–phosphorus distance between two PO_4^{3-} tetrahedra connected by a bridging oxygen. The parameters obtained for the 3Ga-PBG sample are broadly similar to those from the gallium-free sample suggesting that the two materials have similar structures. The main difference is the presence of correlations involving gallium in the data from the 3Ga-PBG sample: the results suggest that the gallium ions are surrounded by 5.9 oxygen atoms at a distance of 1.98 Å and 5.3 phosphorus atoms at a distance of 3.18 Å. These parameters suggest that the Ga^{3+} ions are coordinated by six phosphate groups in the structure and are in good agreement with those of obtained from the EXAFS data. The only notable discrepancy is that the EXAFS-derived Ga–P coordination number of ~2 is significantly lower than the HEXRD-derived value of ~5: this difference is likely to be due to the large errors associated with the EXAFS-derived value caused by multiple scattering, which affects correlations beyond the first coordination shell and was not accounted for in the analysis [40].

The phosphorus–phosphorus coordination numbers derived from the HEXRD data agree within experimental error with those calculated from the ^{31}P NMR data. As expected, the N_{PP} value of 1.5 for the 3Ga-PBG sample is slightly higher than the value obtained of 1.4 for 0Ga-PBG sample, although this difference is not significant if one takes into account the errors associated with these two parameters.

In summary, the results presented here suggest that both materials studied have open structures bases upon short phosphate chains with –OH groups acting as chain-terminating groups. In the gallium-containing sample, the Ga^{3+} ions adopt octahedral coordination. Moreover, the ^{31}P NMR and FTIR data, and the results of the elemental analysis suggest that addition of gallium ethoxide to phosphate-based sol–gel reaction leads to a material with a more consolidated structure, which has greater P–O–P bonding at the expense of –OH groups.

Antibacterial activity

This study was conducted to determine the antibacterial effectiveness of the gallium doped sol–gel glass. The 0Ga-PBG sample was used as a negative control. The results show a net bactericidal effect against *S. aureus* due to the presence of Ga^{3+} ions. The small zone of inhibition seen observed for the 0Ga-PBG control may be due to either a change in pH as the material dissolves or by reduced water activity as ions leach out. These results demonstrate that, as in the case with Ga-doped melt-quenched PBGs [6], Ga-doped sol–gel PBGs also have potential for use in antibacterial devices for biomedical applications.

Conclusions

The sol–gel method to prepare Ga-doped phosphate-based glass presented here represents a significant advancement in the search for new antibacterial materials and leaves the way open for the development of bioresorbable antibacterial coatings for implant devices. Furthermore, comparison of the structure of the Ga-doped material with that of the Ga-free sample suggests that addition of gallium ethoxide to the sol–gel reaction has a significant effect on the structure of the final product, leading to a more consolidated structure with longer phosphate chains. This finding could be of general importance to the development of phosphate-based sol–gel chemistry.

Acknowledgements The authors wish to acknowledge funding from the EPSRC (EP/C000714, EP/C000633 and GR/T21080). We thank STFC for access to the synchrotron and especially Bob Bilsborrow and Mark Roberts of the STFC Daresbury Laboratory for their assistance in the use of stations 16.5 and 9.1, respectively.

References

1. Norrby SR, Nord CE, Finch R (2005) Lancet Infect Dis 5:115
2. Kaneko Y, Thoendel M, Olakanmi O, Britigan BE, Singh PK (2007) J Clin Invest 117:877

3. Olakanmi O, Britigan BE, Schlesinger LS (2000) Infect Immun 68:5619
4. Yan GH, Wang GJ, Li YC (1991) Acta Pharmacol Sin 12:530
5. Harrington JR, Martens RJ, Cohen ND, Bernstein LR (2006) J Vet Pharmacol Ther 29:121
6. Valappil SP, Ready D, Abou Neel EA, Pickup DM, Chrzanowski W, O'Dell LA, Newport RJ, Smith ME, Wilson M, Knowles JC (2008) Adv Funct Mater 18:732
7. Bitar M, Salih V, Mudera V, Knowles JC, Lewis MP (2004) Biomaterials 25:2283
8. Knowles JC (2003) J Mater Chem 13:2395
9. Mulligan AM, Wilson M, Knowles JC (2003) J Biomed Mater Res A 67:401
10. Mulligan AM, Wilson M, Knowles JC (2003) Biomaterials 24:1797
11. Ahmed I, Abou Neel EA, Valappil SP, Nazhat SN, Pickup DM, Carta D, Carroll DL, Newport RJ, Smith ME, Knowles JC (2007) J Mater Sci 42:9827. doi:10.1007/s10853-007-2008-9
12. Pickup DM, Guerry P, Moss RM, Knowles JC, Smith ME, Newport RJ (2007) J Mater Chem 17:4777–4784
13. Liu DM, Yang QZ, Troczynski T (2002) Biomaterials 23:691
14. Achary SN, Jayakumar OD, Tyagi AK, Kulshresththa SK (2003) J Solid State Chem 176:37
15. Walton RI, O'Hare D (2001) J Phys Chem Solids 62:1469
16. Rehr JJ, Albers RC, Zabinsky SI (1992) Phys Rev Lett 69:3397
17. Fletcher DA, McMeeking RF, Parkin D (1996) J Chem Inf Comput Sci 36:746
18. Gorfman S, Tsirelson V, Pucher A, Morgenroth W, Pietsch U (2006) Acta Crystallogr A 62:1
19. Cole JM, van Eck ERH, Mountjoy G, Anderson R, Brennan T, Bushnell-Wye G, Newport RJ, Saunders GA (2001) J Phys Condens Matter 13:4105
20. Gaskell PH (1991) Materials science and technology. VCH, Weinheim
21. Kirkpatrick RJ, Brow RK (1995) Solid State Nucl Magn Reson 5:9
22. MacKenzie KJD, Smith ME (2002) Multinuclear solid-state NMR of inorganic materials. Pergamon-Elsevier, Oxford
23. Shih PY, Ding JY, Lee SY (2003) Mater Chem Phys 80:391
24. Byun JO, Kim BH, Hong KS, Jung HJ, Lee SW, Izyneev AA (1995) J Non-Cryst Solids 190:288
25. Ilieva D, Jivov B, Bogachev G, Petkov C, Penkov I, Dimitriev Y (2001) J Non-Cryst Solids 283:195
26. Baia L, Muresan D, Baia M, Popp J, Simon S (2007) Vib Spectrosc 43:313
27. Orcel G, Phalippou J, Hench LL (1986) J Non-Cryst Solids 88:114
28. Nishi K, Shimizu K, Takamatsu M, Yoshida H, Satsuma A, Tanaka T, Yoshida S, Hattori T (1998) J Phys Chem B 102:10190
29. Charton P, Armand P (2004) J Non-Cryst Solids 333:307
30. Krause M, Gruehn R (1995) Z Kristallogr 210:427
31. Hoppe U, Walter G, Kranold R, Stachel D (2000) J Non-Cryst Solids 263:29
32. Pickup DM, Ahmed I, Guerry P, Knowles JC, Smith ME, Newport RJ (2007) J Phys Condens Matter 19:415116
33. Brow RK (2000) J Non-Cryst Solids 263:1
34. Brinker CJ, Scherer GW (1990) Sol–gel science. Academic Press, London
35. Livage J, Barboux P, Vandenborre MT, Schmutz C, Taulelle F (1992) J Non-Cryst Solids 147:18
36. Nho YC, Kwon OH, Jie C (2002) Radiat Phys Chem 64:67
37. Hoppe U, Ilieva D, Neuefeind J (2002) Z Naturforsch A Phys Sci 57:709
38. Belkebir A, Rocha J, Esculcas AP, Berthet P, Poisson S, Gilbert B, Gabelica Z, Llabres G, Wijzen F, Rulmont A (2000) Spectrochim Acta A 56:423
39. Skipper LJ, Sowrey FE, Pickup DM, Drake KO, Smith ME, Saravanapavan P, Hench LL, Newport RJ (2005) J Mater Chem 15:2369
40. Rehr JJ, Albers RC (2000) Rev Mod Phys 72:621